Supplementary Information

Metallic carbide nanoparticles as stable and reusable substrates for sensitive surface-enhanced Raman spectroscopy

Hua Bai,[a] Wei Liu,[a] Wencai Yi,[b] Xinshi Li,[a] Junfeng Zhai,[a] Junfang Li,[a] Jingyao Liu,*[b] Haifeng Yang,[a] and Guangcheng Xi*[a]

[a]Institute of Industrial and Consumer Product Safety, Chinese Academy of Inspection and Quarantine (CAIQ), No. 11, Ronghua South Road, Beijing 100176, P. R. China.

[b]Laboratory of Theoretical and Computational Chemistry, Institute of Theoretical Chemistry, Jilin University, Changchun 130023, P. R. China.

Correspondence and requests for materials should be addressed to G.C.X. (email: xiguangcheng@caiq.gov.cn) and J.Y.L (email: ljy121@jlu.edu.cn).

Experimental Section

Synthesis of TaC Nanoparticles

All chemicals used in the experiments are analytic purity. In a typical synthesis process, 0.716 g (2 mmol) of anhydrous tantalic chloride ($TaCl_5$) and 2 g of magnesium (Mg) powder were added into 1 mL of absolute ethanol. Then, transferred the mixture to a stainless steel autoclave and sealed this system tightly. **Note:** The above operation is done in a nitrogen-filled glove box. Then the autoclave was heated at 600 °C for 10 h. After the reaction is completed, the autoclave is naturally cooled to room temperature, and the obtained products were collected. The powders were washed three times with hydrochloric acid, perchloric acid, ethanol, and distilled water. Finally, the obtained brown powders were dried at 50 °C in a vacuum drying oven.

Characterization

These samples were measured by a variety characterization techniques. X-ray powder diffraction (XRD) patterns of the products were obtained on a Bruker D8 focus X–ray diffractometer by using CuKα radiation (λ = 1.54178 Å). Scanning electron microscopy (SEM) images and energy-disperse X-ray spectrum (EDS) spectrums were obtained on a Hitachi S-4800. Transmission electron microscopy (TEM), high–resolution TEM (HRTEM) characterizations were performed with a Tecnai G F30 operated at 300 kV. UV–Vis absorption spectra were recorded with a Shimadzu UV3600. The X-ray Photoelectron Spectroscopy (XPS) experiments were performed in a Theta probe (Thermo Fisher) using monochromated Al Kα X-rays at hυ = 1486.6

eV. Peak positions were internally referenced to the C1s peak at 284.6 eV. The Fourier transform infrared (FTIR) spectra were measured from THERMO Iz-10. The specific surface area was measured in a Micro Tristar II 3020. The X-ray photoelectron spectra (XPS) were recorded on an ESCALab-250Xi of ThermoFisher Scientific.

SERS Tests

In order to evaluate the SERS performance of the as-synthesized metallic TaC nanoparticles, a confocal-micro Raman spectrometer (Renishaw-inVia) was used as the measuring instrument. In all SERS tests, if no special statement, the adopted excitation wavelength is always 532 nm, the laser power is 0.5 mW, and the magnification of the objective is × 50 L. A series of standard solutions, such as Rh6G, MO, and 2,4-DCP with concentrations of 10^{-3}-10^{-8} M were adopted as the probe molecules. To improve the signal reproducibility and uniformity, the TaC nanoparticles were dipped into the probe molecule aqueous solution to be measured and maintained for 30 min. After 5 minutes of sonication, the obtained suspension was uniformly coated on a glass slide by spin coating, and then dried in air for 10 min under the irradiation of an infrared light. In all SERS detections, the laser beam is perpendicular to the top of the sample to be tested with a resultant beam spot diameter of 5 μm.

Electronic Structure Calculations

All calculations are performed based on the plane-wave pseudo potential density function theory (DFT), are implemented through Vienna ab initio Simulation Package

(VASP). And the generalized gradient approximation (GGA) with Perdew-Burke-Ernzerh (PBE) functional was employed to describe the electron-ion interactions, where the Ta-$5d^36s^2$ states and the O-$2s^22p^4$ states were treated as valence states. The cutoff energy was chosen at value of 500eV, and Brillouin zones (BZ) integrations were carried using Monkhorst-Pack sampling grids with the mesh of 11×11×11 and 17×17×17 for structure optimizations and DOS calculations, respectively, the high symmetry path was determined generated using A flow software. The atomic positions and lattice constants were optimized using the conjugate gradients (CG) scheme until the force components on each atom were less than 0.02 eV/Å. The face center cubic phase TaC (space group *Fm*-3*m*) was modeled in our calculations and the optimized lattice parameter is a = 4.48 Å.

Enhanced Factor Calculation

To calculate the EF of the TaC nanoparticles, the ratio of SERS to normal Raman spectra (NRS) of RH6G was determined by using the following calculating formula 1

$$EF = (I_{SERS}/I_{NRS}) \times (T_{NRS}/T_{SERS}) \times (C_{NRS}/C_{SERS}) \quad (1)$$

where I_{SERS} and I_{NRS} refer to the peak intensities of the SERS and NRS, respectively. T_{NRS} and T_{SERS} refer to the integration of the NRS and SERS, respectively. C_{NRS} and C_{SERS} refer to the concentrations of the probe molecules of the NRS and SERS, respectively. In the SERS measurements, two Raman scattering peaks, R_1 at 612 cm^{-3} and R_2 at 773 cm^{-3} were selected for the calculations of the EF. For comparison, the peak intensities of the RH6G (1×10^{-3} M, aqueous solution) directly placed on bare glass slide were detected as NRS data. For the NRS data, the integration time is 4000

s, while for the SERS data, the integration time is 10 s.

Supporting Figures

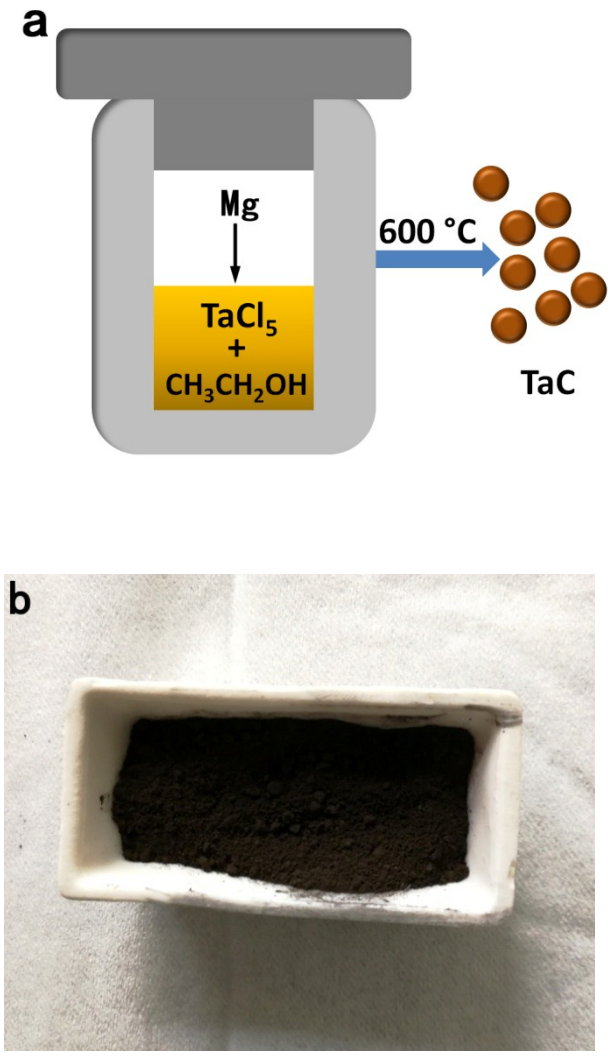

Figure S1. (a) Schematic illustrating the synthesis of the metallic TaC. (b) The photograph of the as-synthesized brown TaC nanoparticles.

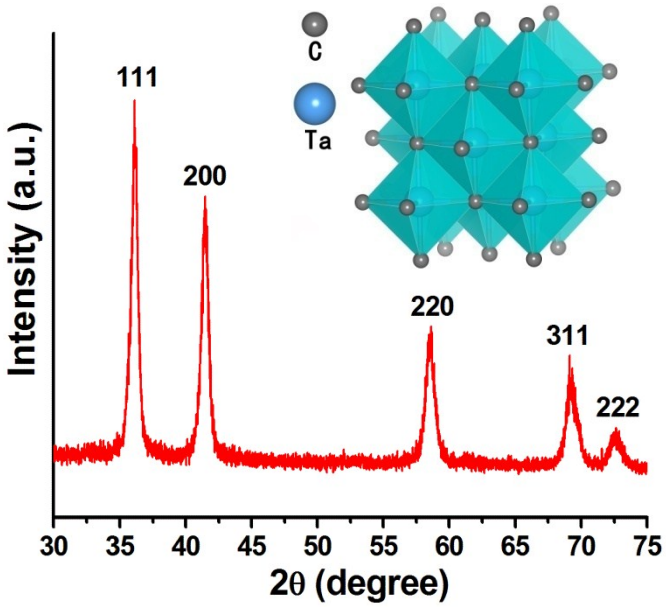

Figure S2. XRD pattern of the prepared TaC sample. inset: crystal structure of face centered cubic TaC.

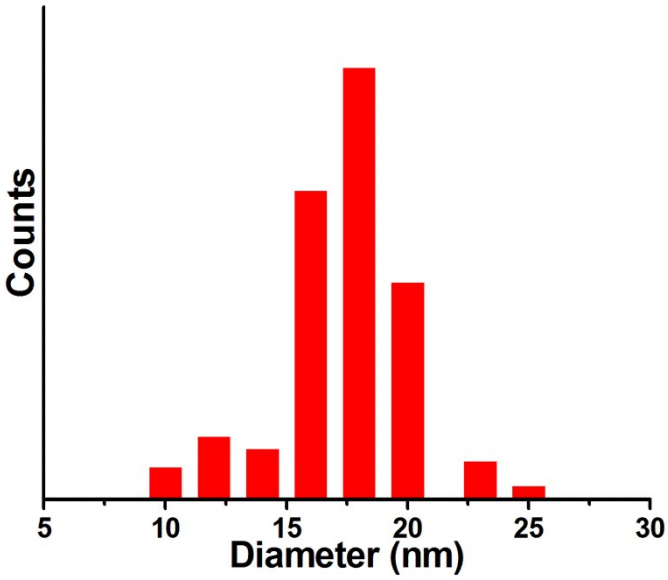

Figure S3. Size distribution of the TaC nanoparticles obtained from the dynamic light scattering measurements.

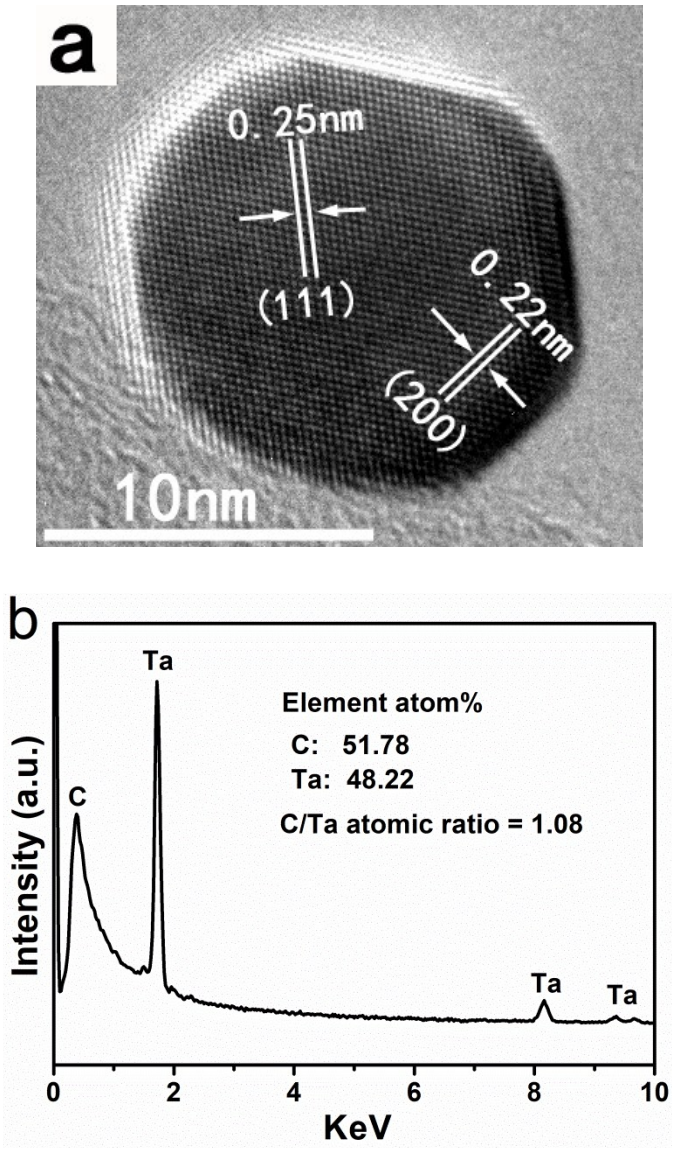

Figure S4. (a) HRTEM image of a TaC particle. (b) EDS component analysis of the sample.

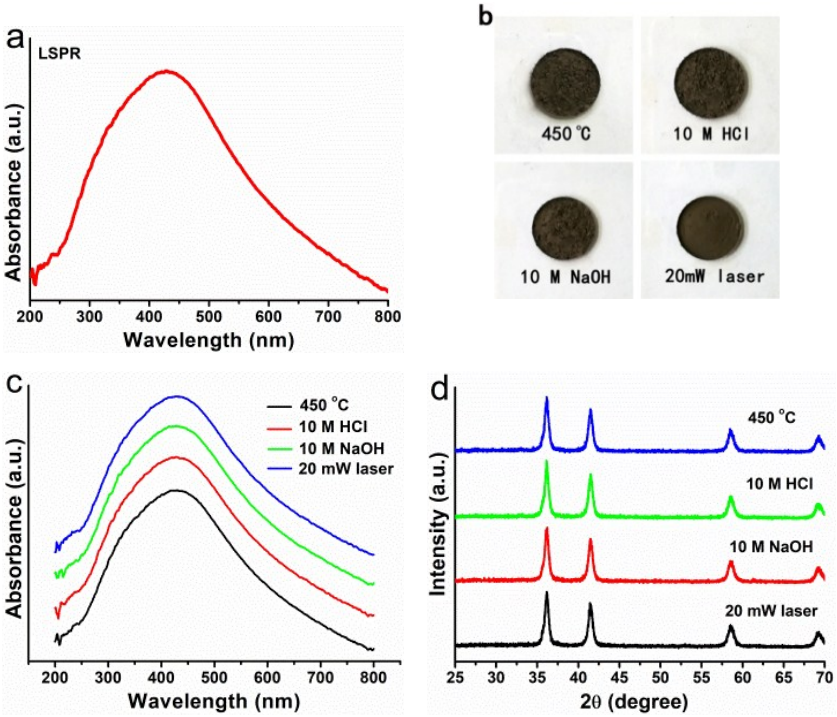

Figure S5. UV-Vis absorption characterizations and the ultrahigh stability of the TaC nanoparticles. (a) UV-Vis absorption spectrum of the sample, showing a strong LSPR peak centered at 429 nm. (b-d) The photographs (b), LSPR peaks (c), and XRD patterns (d) of these samples are almost the same after being heated in air at 450 °C for 5h, corroded with 10 M HCl and NaOH for 10 h, and irradiated by 20 mW laser for 10 h, suggesting the ultrahigh thermal and chemical stability of the TaC nanoparticles.

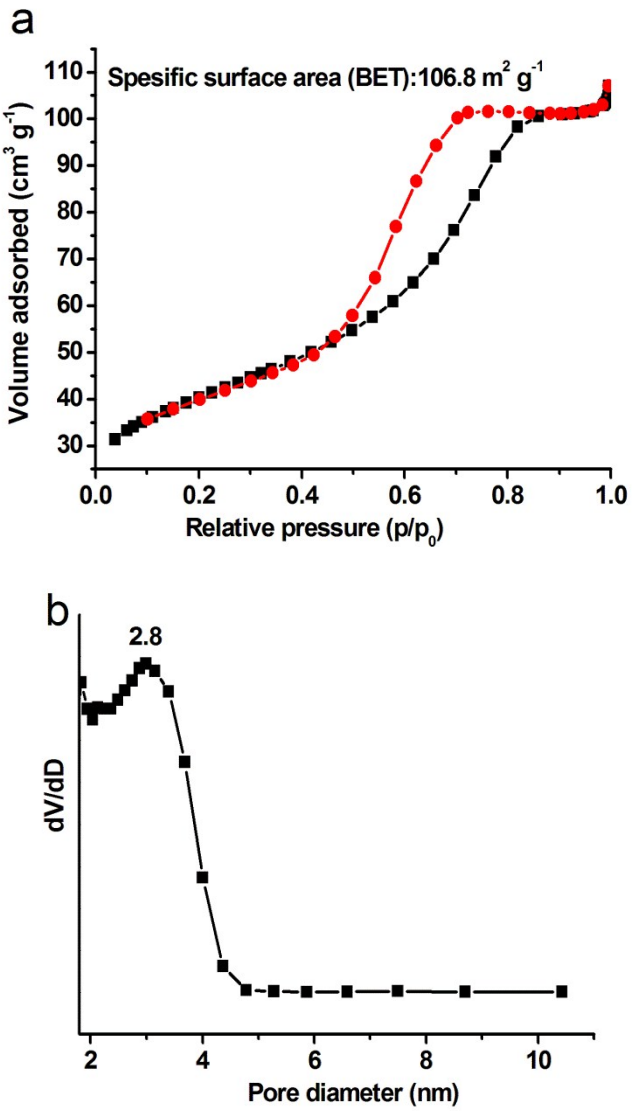

Figure S6. (a) Nitrogen adsorption/desorption isotherms obtained at 77 K. (b) pore size distribution of the sample.

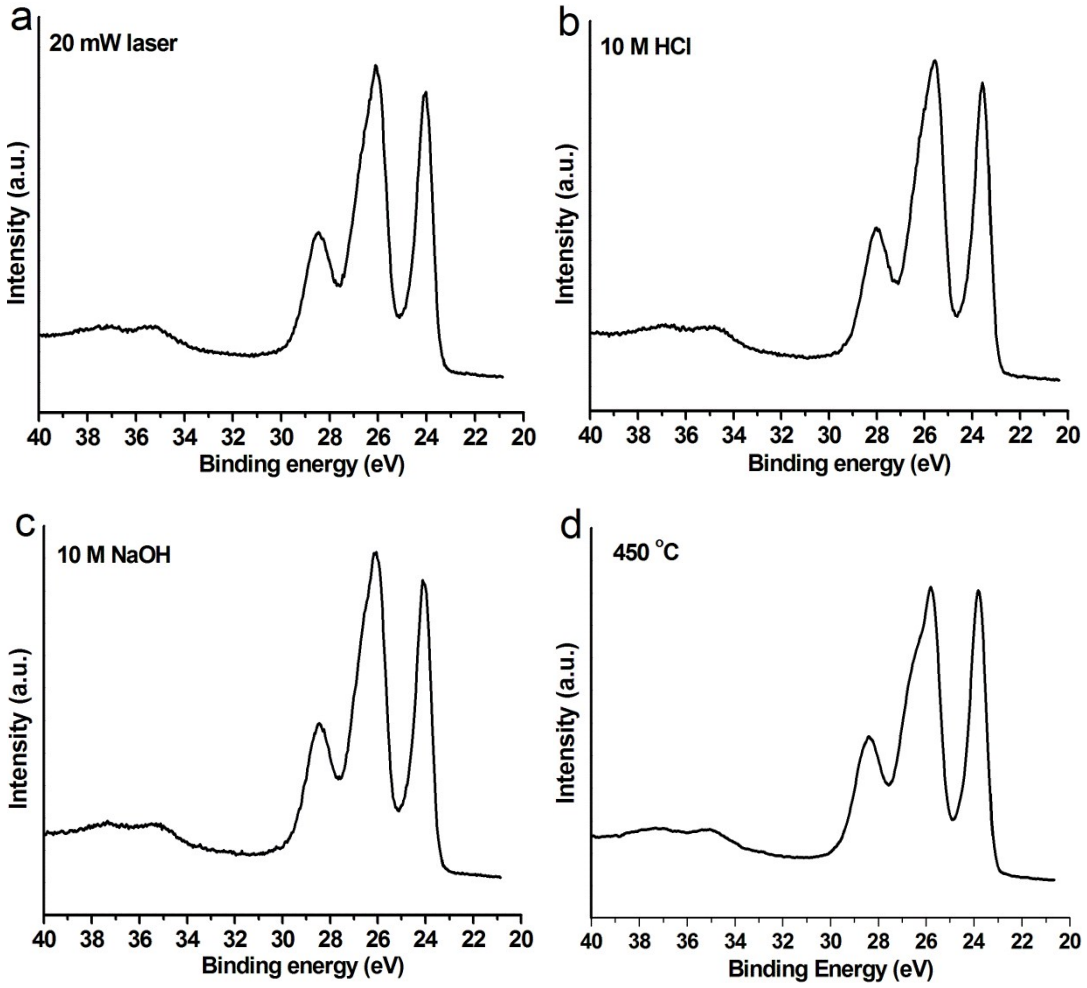

Figure S7. The XPS spectra shown that the oxidation valence of the samples was not changed after (a) laser irradiation, (b-c) acid and alkali corrosion, (d) heating to 450 °C in air, which indicates that the TaC nanospheres have high thermal, oxidation resistance, and corrosion resistance.

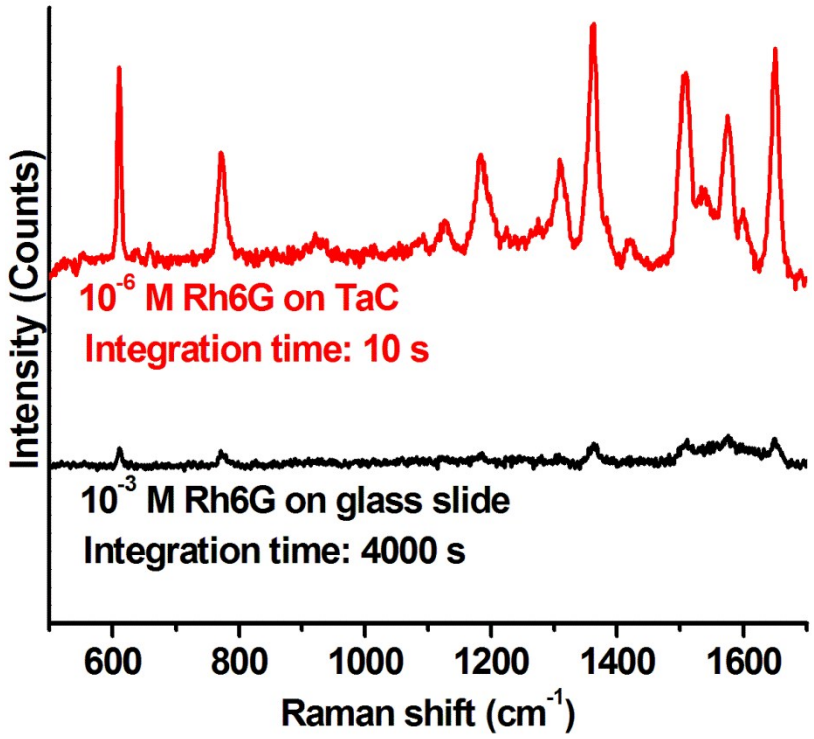

Figure S8. Two Raman spectra were recorded from a 10^{-6} M Rh6G on a TaC nanoparticle substrate and a 10^{-3} M Rh6G on a glass slide, respectively. The estimated enhancement factor is up to 6.4×10^7, which is calculated by 160 (Raman intensity ratio at 612 cm^{-1}) × 1000 (concentration ratio) × 400 (integration time ratio).

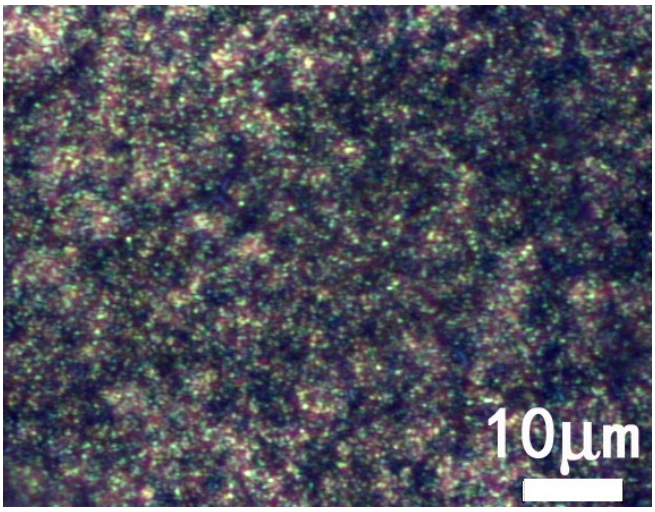

Figure S9. The optical photograph of the TaC nanoparticles SERS substrate fabricated by spin coating, which can be seen that the surface of the formed substrate is very flat and uniform.

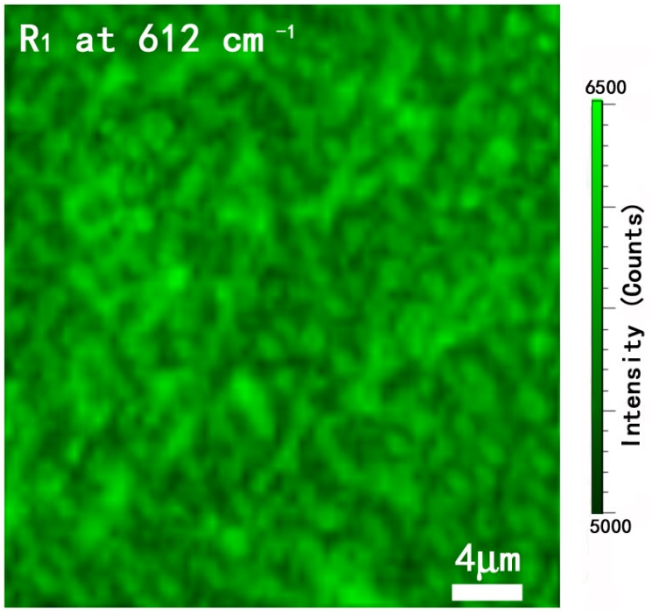

Figure S10. The SERS mapping and intensity distribution of R_1 characteristic peak (612 cm^{-1}) of 10^{-6} M Rh6G.

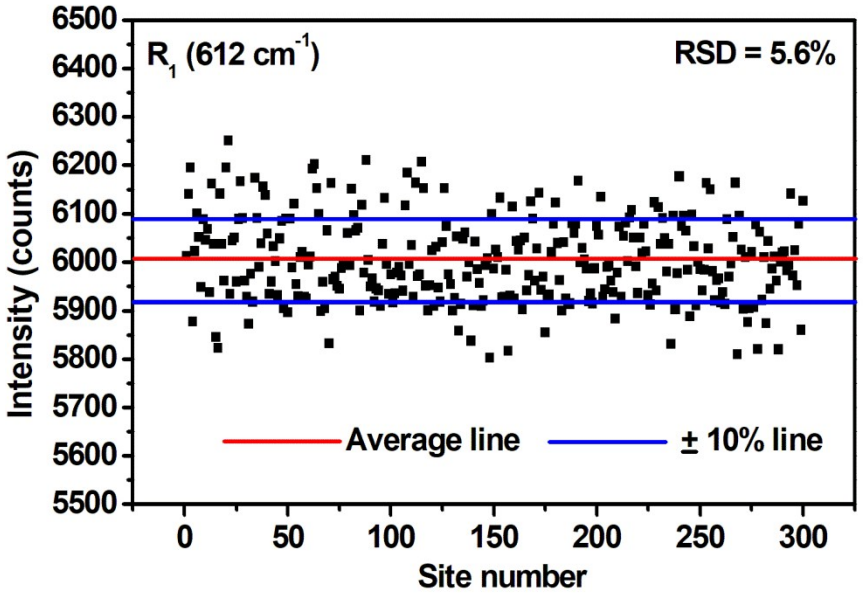

Figure S11. The SERS signal intensities and corresponding RSD at 612 cm^{-1} of 10^{-6} M Rh6G gathered from 300 randomly chosen sites.

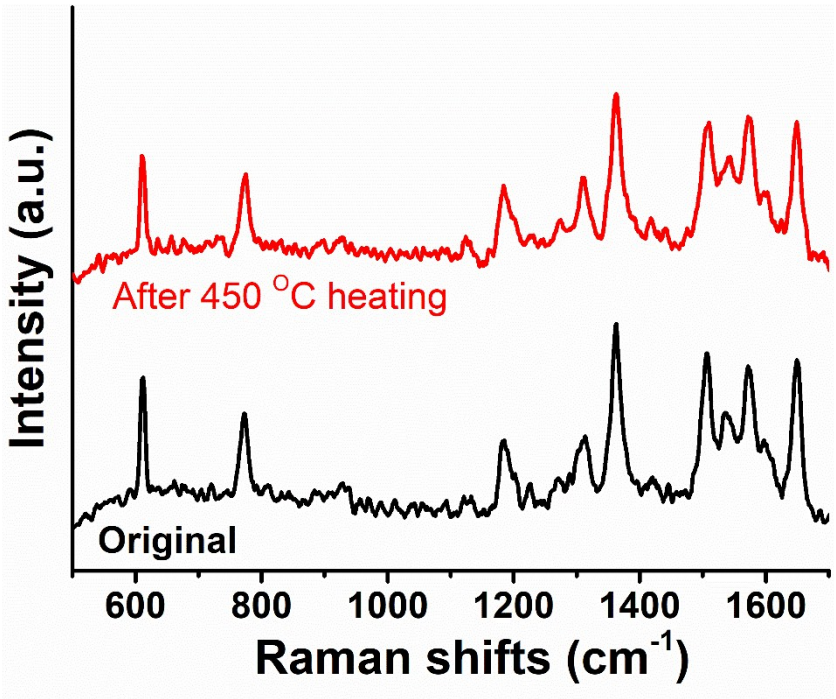

Figure S12. The Raman spectra of the TaC nanoparticles before and after 450 °C heating, which demonstrated that the samples are highly stable.

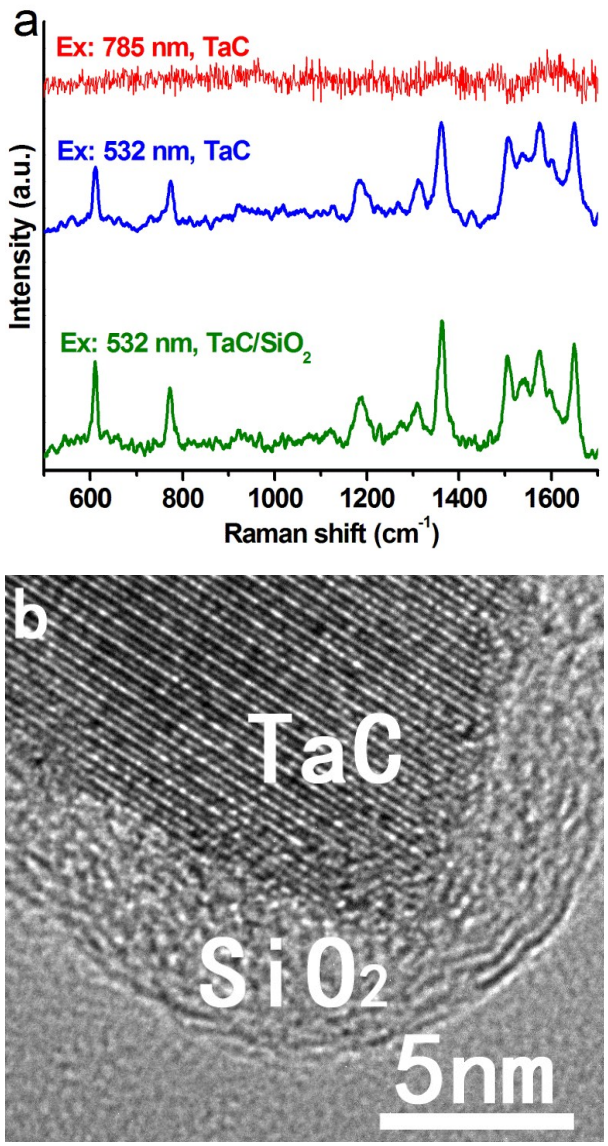

Figure S13. Investigation of SERS enhancement mechanism of the TaC substrate. (a) By changing the excitation wavelength, it is confirmed that the enhancement mechanism of electromagnetic field is playing in the TaC nanoparticles. At the same time, the role of chemical enhancement mechanism was eradicated by covering the surface of TaC nanoparticles with a layer of amorphous SiO_2. (b) HRTEM image of the SiO_2/TaC nanoparticles.

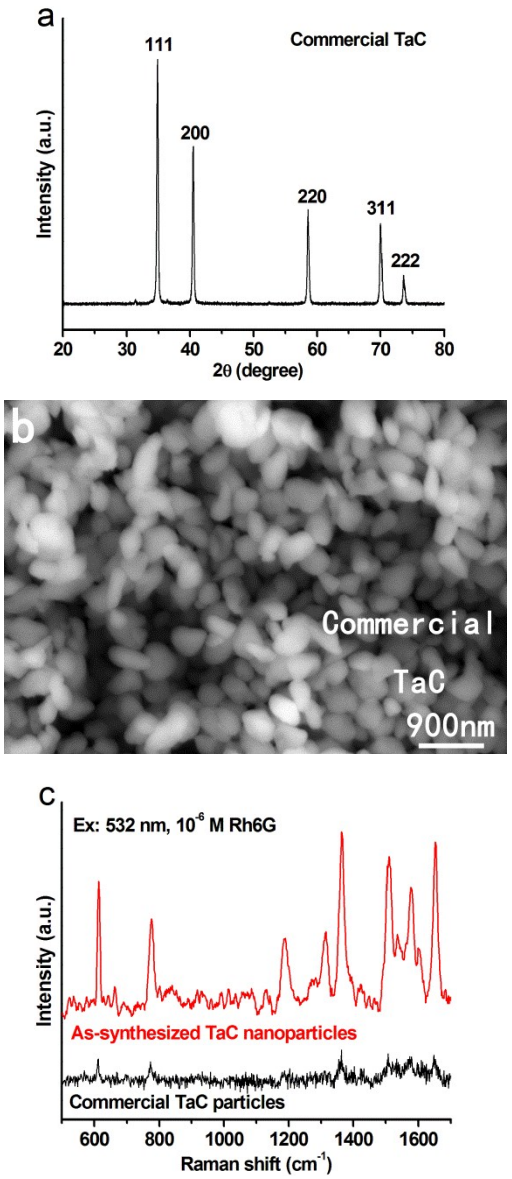

Figure S14. (a-b), XRD pattern and SEM image of the commercial TaC particles. (c) The two Raman spectra obtained on the TaC nanoparticle substrate and commercial particles, respectively.

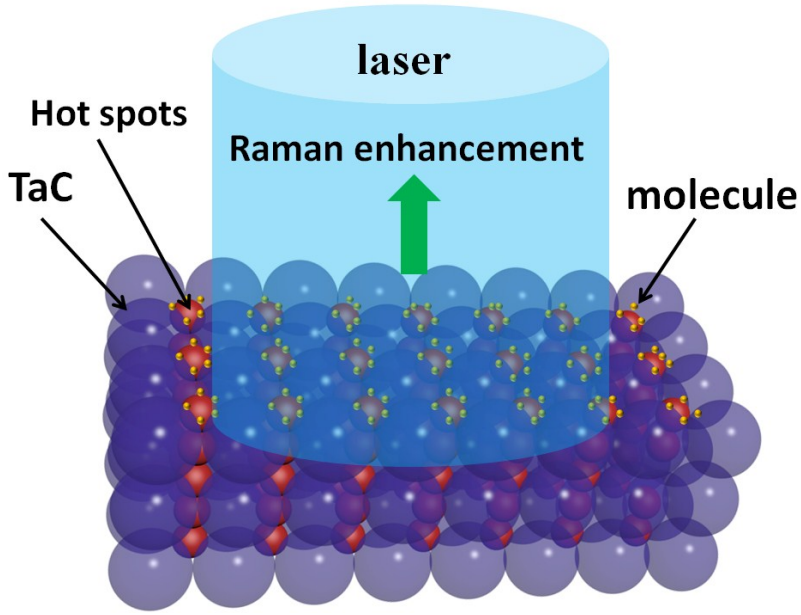

Figure S15. Since the diameter of the as-synthesized TaC nanoparticles is only 15-20 nanometers, the gap between the particles is very small, which creates a lot of "hot spots"; However, due to the diameters of the commercial TaC particles is up to 300-400 nm, the gap between the particles is very large, which greatly reduces the density of the "hot spots".

Table S1: Some of the Previously Reported EFs for Semiconductor Substrates

Material	Probe molecule	**EF**	Excited wavelength (nm)	**Stability**	Author
core–shell TiO_2–Ag	4-Mpy	**6.5×10^5**	514	**easily oxidized**	X. X. Zou et al.[1]
TiO_2 photonic microarray	MB	**2×10^4**	532	**stable**	D. Qi et al.[2]
CdTe nanopartilces	4-Mpy	**10^4**	514.5	**easily oxidized, easy to corrode**	Y. F. Wang et al.[3]
$W_{18}O_{49}$ nanowires	Rh6G	**3.4×10^5**	532.8	**easily oxidized**	S. Cong et al.[4]
CuO nanoparticles	4-Mpy	**10^2**	514.5	**easy to corrode**	Y. Wang et al.[5]
CdS nanoparticels	4-Mpy	**10^2**	514.5	**easily oxidized, easy to corrode**	Y. F. Wang et al.[6]
Cu_2O superstructure	Rh6G	**8×10^5**	674	**easily oxidized, easy to corrode**	J. Lin et al.[7]
Fe_2O_3 nanoparticles	4-Mpy	**2.7×10^4**	514.5	**easy to corrode**	X. Q. Fu et al.[8]
Au–CdSe nanowires	CV	**10^4**	633	**easily oxidized, easy to corrode**	G. Das et al.[9]
Colloidal ZnO	D266	**50**	488	**easy to corrode**	H. Wen et al.[10]
DFH-4T	MB	**3.4×10^3**	785	**easily oxidized, easy to corrode**	Mehmet Yilmaz et al.[11]
TiO_2	Nitrothio Phenol	**10^2**	488	**stable**	Teguh et. al.[12]
ZnO nanorods	4-ABT	**22**	514.5	**easy to corrode**	Kim et. al.[13]
InAs/GaAs quantum dots	Pyridine	**10^3**	514.5	**easily oxidized, easy to corrode**	Quagliano et. al.[14]
H-Si nanowire	Rh6G	**8-28**	532	**easily oxidized**	Wang et. al.[15]

Graphene	Phthalocyanine	**2-17**	632.8	**stable**	Ling et. al.[16]
GaP	CuPc	**700**	514.5	**easily oxidized, easy to corrode**	Hayashi et. al.[17]
WO_2/C nanowires	Rh6G	**1.3×10^6**	532	**stable**	He et al.[18]
MoO_2 nanodumbbells	Rh6G	**3.75×10^6**	532	**stable**	Zhang et al.[19]
MoS_2	Rh6G	**10^6**	532	**easily oxidized, easy to corrode**	Zhao et al.[20]
TaC nanoparticles	**Rh6G**	**6.4×10^7**	**532**	**ultrastable**	**This work**

1 X. X. Zou, R. Silva, X. X. Huang, J. F. Al-Sharabc, T. Asefa, *Chem. Commun.* **2013**, *49*, 382.

2 D. Qi, L. Lu, L. Wang, J. Zhang, *J. Am. Chem. Soc.* **2014**, *136*, 9886-9889.

3 Y. F. Wang, J. H. Zhang, H. Y. Jia, M. J. Li, J. B. Zeng, B. Yang, B. Zhao, W. Q. Xu, *J. Phys. Chem. C*. 2008, *112*,996–1000.

4 S. Cong, Y. Y. Yuan, Z. G. Chen, J. Y. Hou, M. Yang, Y. L. Su, Y. Y. Zhang, L. Li, Q. W. Li, F. X. Geng, Z. G. Zhao, *Nat. Commun*. **2015**, *6*, 7800.

5 Y. Wang, H. Hu, S. Jing. Y. Wang, Z. Sun, B. Zhao, C. Zhao, J. R. Lombardi, *Anal.Sci.* 2007, *23*, 787–791.

6 Y. F. Wang, Z. H. Sun, Y. X. Wang, H. L. Hu, B. Zhao, W. Q. Xu, J. R. Lombardi, *Spectrochimica*. *Acta*. *Part*. *A*. 2007, *66*, 1199–1203.

7 J. Lin, Y. Shang, X. X. Li, J. Yu, X. T. Wang, L. G. *Adv. Mater*. **2017**, *29*, 1604797.

8 X. Q. Fu, F. L. Bei, X. Wang, X. J. Yang, L. D. Lu, *J. Raman Spectrosc.* **2009**, *40*,

1290–1295.

9 G. Das, R. Chakraborty, A. Gopalakrishnan, D. Baranov, E. D. Fabrizio, R. Krahne, *J Nanopart Res*. **2013**, *15*, 1596.

10 H. Wen, T. J. He, C.Y. Xu, J. Zuo, F. C. Liu, *Molecular Physics*. 1996, *88*, 281–290.

11 M. Yilmaz, E. Babur, M. Ozdemir, R. L. Gieseking, Y. Dede, U. Tamer, G. C. Schatz, A. Facchetti, H. Usta, G. Demire, *Nat. Mater.* **2017**, DOI: 10.1038/NMAT4957.

12 J. S. Teguh, F. Liu, B. Xing, E. K. L. Yeow, *Chem. Asian J*. **2012**, *7*, 975.

13 K. Kim, K. L. Kim, K. S. Shin, *Phys. Chem. Chem. Phys*. **2013**, *15*, 9288.

14 L.G. Quagliano, *J. Am. Chem. Soc*. **2004**, *126*, 7393.

15 X. Wang, W. Shi, G. She, L. Mu, *J. Am. Chem. Soc.* **2011**, *133*, 16518.

16 X. Ling, L. Xie, Y. Fang, H. Xu, H. Zhang, J. Kong, Mi. S. Dresselhaus, J. Zhang, Z. F. Liu, *Nano Lett.* **2010**, *10*, 553.

17 S. Hayashi, R. Koh, Y. Ichiyama, K. Yamamoto, *Phys. Rev. Lett.* **1988**, *14*, 1085.

18 C. Y. He, H. Bai, W. C. Yi, J. Y. Liu, X. S. Li, X. Li, G. C. Xi, *J. Mater. Chem. C* **2018**, *6*, 3200-3205.

19 Q. Q. Zhang, X. S. Li, Q. Ma, Q. Zhang, H. Bai, W. C. Yi, J. Y. Liu, J. Han, G. C. Xi, *Nat. Commun*. **2017**, *8*, 14903.

20 Z. H. Zheng, S. Cong, W. B. Gong, J. N. Xuan, G. H. Li, W. B. Lu, F. X. Geng Z. G. Zhao, *Nat. Commun.* **2017**, *8*, 1993.